1 Application of the Jellium Model and its Refinements to the Study of the Electronic Properties of Metal Clusters

WALTER EKARDT

Fritz-Haber-Institut der Max-Planck-Gesellschaft, Berlin,

W.-D. SCHÖNE

Fritz-Haber-Institut der Max-Planck-Gesellschaft, Berlin

and

J. M. PACHECO

Departamento de Física da Universidade, Coimbra

1.1 INTRODUCTION

The jellium model, known from the study of the electronic properties of NFE (nearly free electron) metals [1] and from the understanding of the electronic properties of free metallic surfaces [2], is applied to the calculation of the electronic properties of metal clusters, mainly to the group Ia (alkaline metals) and to the group Ib metals (noble metals).

Metal Clusters. Edited by W. Ekardt

The model is shown to give results that are very often in *quantitative* agreement with experimental data and serve in most other cases as a good starting point for the calculation of the effects of the ionic structure, e.g. via pseudopotential perturbation theory.

Main experimental findings both for the ground state (magic numbers for the stability of clusters [3] and the existence of supershells [4]) and for excited states (the dominance of collective states in the photoabsorption of metal clusters Me_N with $N > 8$) were *predicted* [5] before their experimental confirmation. Recently we were able to explain the temperature dependence of the absorption of small metal clusters as observed by Haberland's group [6]. If the model is complemented by pseudopotential perturbation theory [7] the results obtained match *qualitatively* those obtained by demanding quantum-chemical methods (e.g. the photoabsorption spectra of Na_6). Further improvement of the model includes the removal of self-interaction effects, the so-called SIC [8–10] (a consequence of using the local density approximation (LDA) to general density functional theory (DFT)).

The development of the *super-atom model* for the description of electronic properties of metal clusters arose from the attempt to understand and interpret experimental data by W. Schulze and co-workers Figure 1.1 shows the absorption of small silver particles

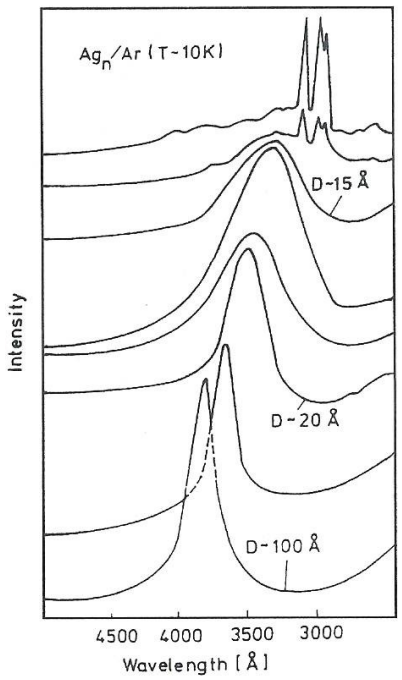

Figure 1.1 Optical absorption of small silver particles Ag_N embedded in argon at low temperatures, according to Ref. [11]. The huge absorption hump is a collective electronic oscillation localized at the interface Ag/Ar. This figure historically gave the impact for the development of the super-atom model for metal clusters. For large clusters a broad, damped peak is observed, whereas for small clusters the line is fragmented

(in arbitrary units) as a function of wavelength with the mean diameter of the clusters as parameter. As one can see, there is a pronounced blue-shift of the absorption hump as the cluster size decreases. If one tries to understand the observed absorption within *classical, macroscopic electrodynamics*, one has to look at the imaginary part of the dynamical polarizability of a small metal particle embedded in a dielectric host. The textbook solution for a spherical particle of radius R is [12]

$$\alpha(\omega) = R^3 \frac{\varepsilon(\omega) - \varepsilon_d(\omega)}{\varepsilon(\omega) + 2\varepsilon_d(\omega)}, \tag{1}$$

where $\varepsilon(\omega)$ and $\varepsilon_d(\omega)$ are the dielectric constants of bulk silver and the dielectric host, respectively. As in the case of bulk plasmons, defined in terms of the vanishing of $\varepsilon(\omega)$, collective interfacial excitations are characterized by the vanishing of the denominator, which means that there is an eigenoscillation *in the absence of external stimuli* [13]. Since both dielectric constants are size-independent, one sees immediately that classical, macroscopic electrodynamics does *not* work in this size regime. Therefore one has to resort to *microscopic or mesoscopic models*.

The first, most primitive, model is the infinite barrier model (IBM). Here the electronic motion is confined by a spherical potential hole with infinitely high barriers. Once the electronic wave functions (spherical Bessel functions) and eigenvalues are known, one can proceed and calculate the dynamic polarizability $\alpha(\omega)$. From this quantity the collective excitations are determined in a straightforward manner (see below). The theoretical prediction [50], shown in Figure 1.2, matches the experimental data (indicated by dots) rather well from very small to mesoscopic particle sizes. The result obtained shows that the IBM, which models the kinetic repulsion of the occupied 4d-shell of atomic Xe, works surprisingly well. This repulsion causes an *enhanced* electronic density, leading to the blue-shift of the surface-plasmon line.

For the description of *free* metal clusters, as observed and investigated in supersonic beams, the electrons relax (and tunnel) into the neighboring vacuum. In order to model

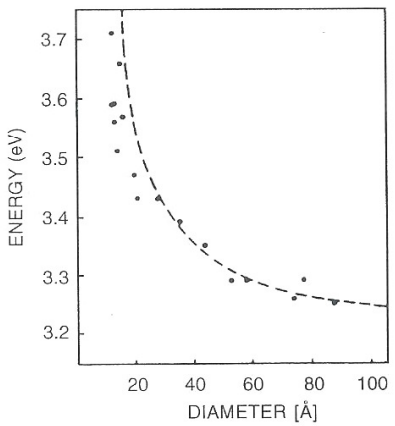

Figure 1.2 Crude theoretical interpretation of the experimental data of Figure 1.1. Here the electronic motion is confined by the IBM (infinite barrier model). For details see the original work by Ekardt *et al.* [50]. Reprinted by permission of Elsevier Science Publishers

this situation, it is useful to recall the series of papers by N. D. Lang and W. Kohn [14, 2], who applied the *self-consistent jellium model* to the study of the electronic properties of free metallic surfaces. A study along this line provides a first *qualitative* understanding of these properties, which is often even *quantitatively* correct (in the case of some alkali metals), and serves in all cases as a good starting point for refined models [15, 16]. As the defining property of a metal cluster is the very existence of its *surface*, the jellium model can be expected to produce good first-order results for clusters as well. These can be improved, if necessary, by pseudopotential perturbation theory to include the effects of the ionic structure (see below). Without any detailed calculation one can predict that the relaxation of the electronic cloud leads to a reduced density, and this in turn to a red-shift of the surface-plasmon line. Therefore, if this were the only active mechanism (as in the alkalines) and if there were *no* complications because of the dynamical coupling to d-electrons, as in Ag, one can immediately predict the experimentally observed red-shift of the surface-plasmon frequency of free alkaline metal clusters. In contrast, the surface-plasmon of neutral Ag-clusters in a molecular beam undergoes a *blue-shift* [17]. Most probably this is the effect of dynamical coupling to d-electrons. The frequency position of the plasmon of the s-electrons cannot be understood without taking into account their dynamical coupling to the d-electrons [13, 18]. For Ag *clusters*, there is the additional complication of the size-dependent hybridization between s and d electrons, respectively.

In this work we start with the primitive jellium model, as appropriate for alkaline metals. In the jellium model for metal clusters a fundamental input is the *size-dependent* ionic density. Fortunately, when one of us started this calculation in 1984 [3], some experimental data about the size dependence of the nearest-neighbor distance were available from EXAFS (extended X-ray absorption fine structure) measurements [19]. Except for fine details the size dependence is very weak. This means that in a first approximation the bulk density of the metal can be used as input for a cluster calculation. A second question is the size dependence of the *shape*. Since electron micrographs very often show a spherical shape, at least for the larger clusters, a spherical shape will be assumed for all cluster sizes. This means that for monovalent systems the radius R of the jellium cluster is determined by its bulk density n_+,

$$\frac{1}{n_+} = \frac{4\pi}{3} r_s^3 = \frac{1}{N} \frac{4\pi}{3} R^3, \tag{2}$$

where r_s is the Wigner–Seitz radius of the electron gas and N is the number of *delocalized* valence electrons within the cluster.

1.2 PROPERTIES OF THE GROUND STATE

The properties of metal clusters within the jellium model were first studied within the local density approximation (LDA) to the density functional theory (DFT) [3]. This means the following set of equations has to be solved self-consistently, starting from a proper initial density (for details see [3]). The total electronic density $\rho(\boldsymbol{r})$ obeys the subsidiary condition

$$\int \rho(\boldsymbol{r})\, \mathrm{d}\boldsymbol{r} = N, \tag{3}$$

where ρ is found by minimizing the total energy functional $E_{\text{tot}}[\rho]$ [20]:

$$E_{\text{tot}}[\rho] = \int \mathrm{d}\boldsymbol{r} v_{\text{ex}}(\boldsymbol{r})\rho(\boldsymbol{r}) + G[\rho], \tag{4}$$

$$G[\rho] = E_{\text{kin}}[\rho] + E_{\text{es}}[\rho] + E_{\text{xc}}[\rho]. \tag{5}$$

E_{kin} describes the kinetic energy of the system of correlated electrons, E_{es} the classical Coulomb repulsion and E_{xc} the exchange–correlation energy. The traditional approximation to the unknown exchange–correlation part of the functional is the local density approximation [21]. The exact density, which determines the total energy in the ground state, is found by solving the Kohn–Sham equations [21]

$$\left(-\frac{\hbar^2}{2m}\Delta + v_{\text{eff}}[\rho(\boldsymbol{r})]\right)\psi_i(\boldsymbol{r}) = \varepsilon_i\psi_i(\boldsymbol{r}), \tag{6}$$

where the electronic density $\rho(\boldsymbol{r})$ is given by

$$\rho(\boldsymbol{r}) = 2\sum_{i=1}^{N}|\psi_i(\boldsymbol{r})|^2. \tag{7}$$

N is again the number of valence electrons and the factor of 2 accounts for the spin degeneracy. If the Gunnarsson–Lundqvist parameterization for the exchange and correlation potential is used [22], the effective potential v_{eff} is given (in Rydberg atomic units) by

$$v_{\text{eff}}(\boldsymbol{r}, \rho) = v_{+}^{\text{JBG}}(\boldsymbol{r}) + 2\int \mathrm{d}\boldsymbol{r}'\frac{\rho(\boldsymbol{r}')}{|\boldsymbol{r}-\boldsymbol{r}'|} - \frac{1.222}{r_{\text{s}}(\boldsymbol{r})} - 0.0666\ln\left(1+\frac{11.4}{r_{\text{s}}(\boldsymbol{r})}\right). \tag{8}$$

$v_{+}^{\text{JBG}}(\boldsymbol{r})$ is the external potential caused by the positive jellium background. The Wigner–Seitz radius $r_{\text{s}}(\boldsymbol{r})$ is obtained by

$$r_{\text{s}}(\boldsymbol{r}) = \left(\frac{4\pi\rho(\boldsymbol{r})}{3}\right)^{\frac{1}{3}}. \tag{9}$$

This set of equations has to be solved *self-consistently*, with some suitable initial density (for numerical details see [3]). This was done first for sodium as a function of the number of atoms N (which agrees with the number of delocalized electrons for monovalent metals). The set of equations was solved for $N = 2, 3, 4, \ldots$ up to 254. Figures 1.3 and 1.4 show typical charge densities and potentials for a small ($N = 20$) and a large ($N = 198$) particle number, respectively. The oscillatory electronic charge density is normalized to the constant background charge (the step-edge in the figures), and the continuous lines depict the occupied levels. The quantum numbers are those of a spherical potential. Hence the bottom level is 1s, followed by 1p, 1d and 2s (for $N = 20$) with the usual meaning of s ($l = 0$), p ($l = 1$) and d ($l = 2$) in terms of the angular momentum l. The level scheme transforms from a pronounced discrete structure, reminiscent of an atomic system, to the quasicontinuum of a mesoscopic system. Since level structure and nomenclature are like those of a very large atom this model was termed the *super-atom model* of metal clusters.

The first physical quantity of interest is the size dependence of the binding energy

$$\delta(N) = \frac{E(N) - NE(1)}{N}, \tag{10}$$

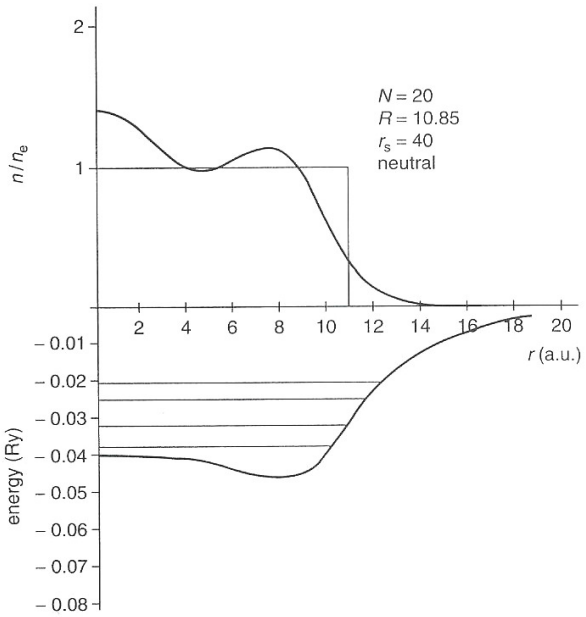

Figure 1.3 Electronic charge density, effective potential and occupied levels for Na_{20} as obtained within the jellium model. The electronic charge density is normalized to a constant ionic background (step-edge). For further explanation see text. Reproduced with permission from Reference [3]. Copyright 1984 by the American Physical Society

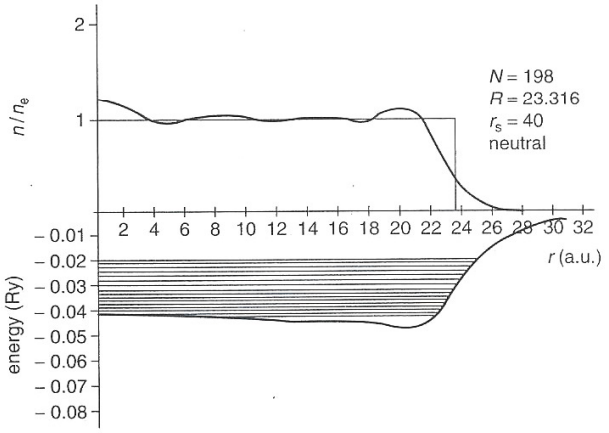

Figure 1.4 Same as Figure 1.3 but for Na_{198}. Comparing with Figure 1.3 one clearly sees how the system transforms from a discrete atomic-like level structure to the quasicontinuum of a mesoscopic system. Reproduced with permission from Reference [3]. Copyright 1984 by the American Physical Society

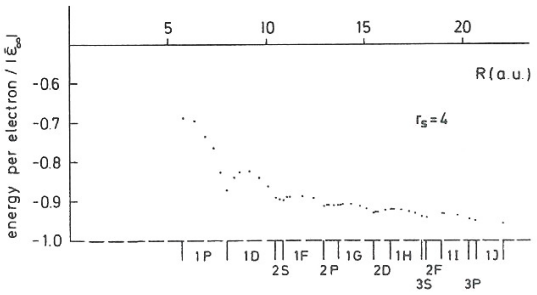

Figure 1.5 Total energy $E(N)/N$ for Na clusters. The pronounced dips at $N = 2$, 8, 20, 40, 58 and 92 constitute so-called *magic numbers*, indicating especially stable cluster sizes. While small magic numbers coincide with shell-closings, the situation is different for larger numbers. For more explanation see text. Reproduced with permission from Reference [3]. Copyright 1984 by the American Physical Society

which requires the calculation of the total energy as a function of size N, with the Wigner–Seitz radius r_s as a parameter. Figure 1.5 shows the quantity $E(N)/N$ in units of its limiting value for $N \to \infty$ for the case of Na. The most remarkable property of this result is that the value at infinity is approached not in a monotonic but in a pronounced oscillatory fashion. In order to show the origin of this property more clearly, the bottom line indicates the symmetry of the top level, i.e. of the shell that is being filled. Looking at *small* particle numbers, one is tempted to conclude that these 'magic numbers' simply result from the closing of the spherical shell (hence $N = 2$, 8, 20, etc. are expected to be magic). That this conclusion is (at least *generally*) wrong can be seen by looking at *medium-size* numbers N. For instance, between $N = 58$ (closed 1g shell) and $N = 92$ (closed 3s shell) there are two more shell-closings (2d at $N = 68$ and 1h at $N = 90$), that do not produce magic numbers. Therefore one can state that the closing of a spherical shell is a necessary but not sufficient condition for the existence of magic numbers. By inspection of the single-particle level structure one easily recognizes that magic numbers are accompanied by especially large gaps between the highest occupied and the lowest unoccupied molecular orbital, the so-called HOMO–LUMO gaps. This property is genuine for the jellium model.

Two features of the jellium description of the super-atom model are experimentally confirmed:

(a) The detailed geometrical structure of the ionic skeleton is of marginal importance [23].
(b) The central property of the model, namely the quasifree motion of the delocalized electrons and especially their mutual correlation is *the* essence for the stability of metal clusters of this kind (all group Ia (alkali metals) and Ib (noble metals) and in addition a few divalent and three-valent metals.

These predictions made in February 1984 have been experimentally confirmed by pioneering experiments of the Berkeley group in June 1984 (see Figure 1.6) [24]. Whereas W. Knight in his early 1984 experiments focused on small mass numbers, these mass-abundance spectra have been afterwards extended to larger atomic numbers. S. Bjørnholm [23] was able to confirm that all magic numbers found for $N \leq 1000$ are those of the jellium model (Figure 1.7). Notice the *absence* of magic numbers between $N = 58$

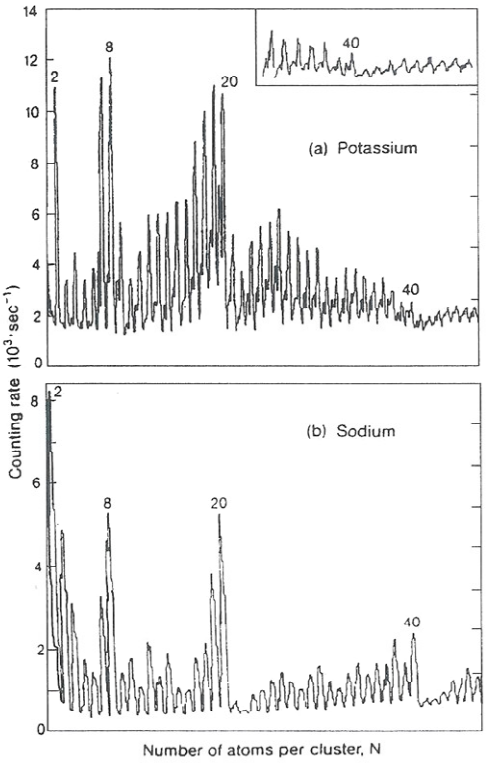

Figure 1.6 Early mass-abundance spectrum of the Berkeley group [27]. Magic numbers are clearly identified. Substructures between the main magic numbers were later sufficiently well explained within the deformed jellium model by Keith Clemenger [28] and Ekardt and Penzar [29]

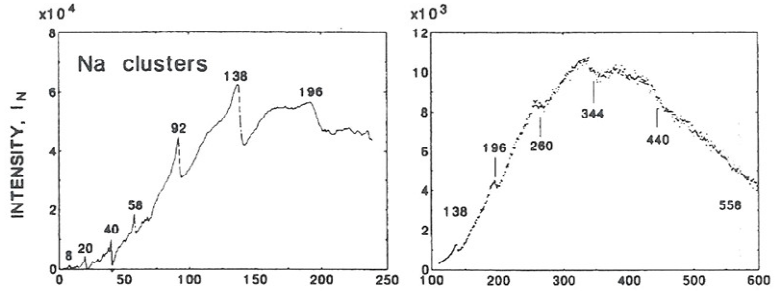

Figure 1.7 Experimental mass spectra by Bjørnholm *et al.* [23] for several hundreds of Na atoms. Note the *absence* of magic numbers between 58 and 92 and between 92 and 138. This can be considered as a direct confirmation of the jellium approximation. Reproduced with permission from Reference [23]. Copyright 1990 by the American Physical Society

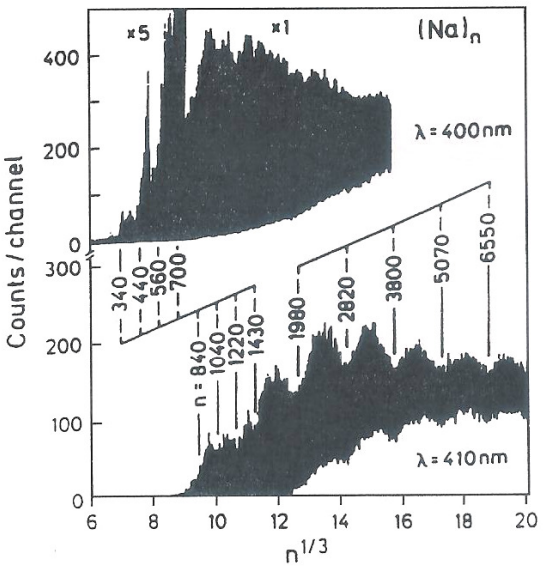

Figure 1.8 Experimental mass spectra of Na up to $N = 22\,000$ [25]. All magic numbers up to $N = 1500$ can be understood within the jellium model and it is only for still larger atomic numbers that the mass anomalies can be attributed to the formation of *ionic* shells. Reproduced by permission of Springer-Verlag from Reference [25]. Copyright by Springer-Verlag

and $N = 92$. In 1991 T. P. Martin [25] was able to take mass spectra for sodium clusters for up to 22 000 atoms, with the remarkable result that all magic numbers $N \leq 1500$ could be explained within the framework of the super-atom model. It is only for even larger N that mass anomalies (see Figure 1.8) could be related to *atomic rearrangements* [25].

The next physical quantities of interest are the size dependence of the ionization potential and of the electron affinity because these quantities can be related to the chemical reactivity of metal clusters. Within the DFT jellium model the size dependence of the ionization potential is easily obtained from two total energy calculations:

$$\Delta_{\mathrm{IP}}[N] = E^{+}[N-1] - E^{0}[N]. \tag{11}$$

Here $E^{+}[N-1]$ denotes the total energy of a positively charged cluster with $N-1$ electrons and $E^{0}[N]$ the total energy of the neutral system. Since the total energy functional consists of various pieces (see Eqs (4) and (5)) this quantity can be written as follows:

$$\Delta_{\mathrm{IP}}[N] = \Delta_{\mathrm{es}} + \Delta_{\mathrm{rest}}. \tag{12}$$

For $N \to \infty$ the first term tends to the electrostatic dipole barrier $v_{\mathrm{es}}(+\infty) - v_{\mathrm{es}}(-\infty)$, i.e. the difference between the electrostatic potentials far outside and deeply inside the metal, and the second term equals the chemical potential. In this limit Δ_{IP} is the work function of the solid [2].

Figure 1.9 shows the theoretical results for $\Delta_{\mathrm{IP}}[N]$ and Δ_{es} for the case of Na together with the limiting values of the work function (3.02 eV) and the electrostatic surface barrier (0.98 eV), respectively (dashed lines). Whereas $\Delta_{\mathrm{IP}}[N]$ shows large discontinuities

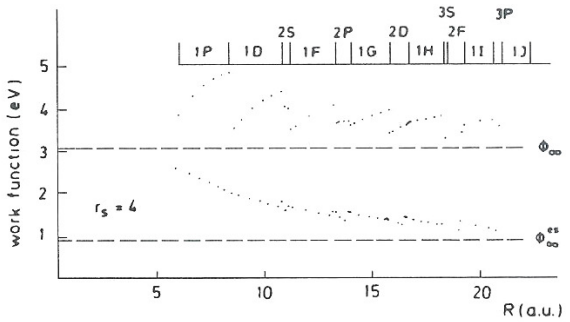

Figure 1.9 Ionization potential for Na clusters in the jellium model [3]. Notice that the total ionization potential does not approach the bulk value in a monotonic fashion but with a pronounced sawtooth behavior. In contrast, the electrostatic part of the total IP *is* monotonic. Here the two horizontal dashed lines represent, respectively, the total work function of the infinite half-space Φ_∞ and the electrostatic surface barrier Φ_∞^{es}. Reproduced with permission from Reference [3]. Copyright 1984 by the American Physical Society

at shell-closings, Δ_{es} is smooth and approaches the limiting value in a monotonic way. Δ_{es} corresponds to the additional amount of work required for ionizing the finite piece of metal and is approximately given by $e^2/(2R)$, the classical electrostatic self energy of one surface charge. This close agreement is related to the fact that also quantum-mechanically the remaining charge is confined mainly to the surface region, except for fine details originating from Friedel oscillations [3, 26].

Experimental data for the ionization potential (IP) are shown in Figure 1.10 [27]. The ionization potential shows large even–odd oscillations for *small* particle numbers, but no pronounced sawtooth patterns for medium-size numbers, in contrast to the theoretical predictions. This suggests that an important ingredient is lacking in the model. Indeed,

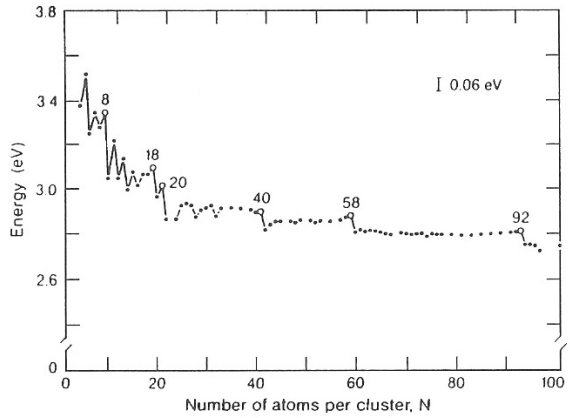

Figure 1.10 Experimental ionization potential (IP) of K clusters [27]. Note that the total IP shows strong discontinuities at magic numbers, whereas the predicted rise of the IP between two magic numbers is missing. As has been shown by Penzar and Ekardt [31] this can be reproduced within the self-consistent deformed jellium model. Reproduced by permission of Academic Press

noticing that at *spherical* shell-closing, the predicted *strong* discontinuities in the IP *are* experimentally confirmed, one realizes that for any *open* shell (all numbers except magic ones) the electronic charge density is non-spherical, a situation that can give rise to a Jahn–Teller distortion of the jellium nucleus. K. Clemenger [28] was the first to study spheroidal distortions of the jellium sphere by using the non-self-consistent Nilsson model of nuclear structure theory. His work was quickly followed by a complete self-consistent many-body calculation for the study of two-axial distortions of the jellium sphere [29]. Brack [30] was the first to study three-axial distortions of the jellium nucleus by using ideas from nuclear structure theory. If one includes these axial distortions one can successfully explain both the ionization potential and the electron affinity for open-shell clusters [30, 31]. Furthermore, fine details of the mass-abundance spectra are better understood.

In order to better understand the origin of the spheroidal distortion, let us recall the appearance of the electronic charge density for any particle number N,

$$\rho(\boldsymbol{r}) = 2 \sum_{n_l, l, m} |Y_{l,m}(\theta, \phi)|^2 |R_{n_l,l}(r)|^2. \tag{13}$$

Because of the relation

$$\sum_{m=-l}^{m=+l} |Y_{l,m}(\theta, \phi)|^2 = \frac{1}{4\pi}, \tag{14}$$

the total electronic charge density is *non-spherical* for all particle numbers except the magic numbers. According to general rules of quantum mechanics, a Jahn–Teller deformation of the external field is to be expected. This is efficiently achieved by introducing the distortion parameter δ describing the replacement of a sphere with radius R by a spheroid whose axes are given by

$$Z = \left[\frac{2+\delta}{2-\delta}\right]^{2/3} R,$$

$$X, Y = \left[\frac{2-\delta}{2+\delta}\right]^{1/3} R. \tag{15}$$

The introduction of δ makes the external potential axial symmetric. Consequently, the spherical symmetry of the wave functions is replaced with a spheroidal symmetry. As before, the radius R is determined by the particle number N and the Wigner–Seitz radius r_s as follows:

$$R = N^{1/3} r_s. \tag{16}$$

The total effective potential determining the electronic motion via the Kohn–Sham equations is expected to be spheroidal as well. Therefore all spherical shells n, l, m are expected to split into spheroidal subshells $|m|, p, k$. Here m is the preserved azimuthal quantum number. For time-reversal symmetry only its magnitude $|m|$ counts; p is the parity and k just enumerates the levels of a certain symmetry. The reduced spheroidal symmetry lifts the spherical degeneracy as depicted in Figure 1.11 for Na in the size-range of N from 3 to 18.

An immediate consequence of this spheroidal nature of the one-particle Kohn–Sham levels is the substructuring of the formerly spherical shells into spheroidal subshells. This is made evident in Figures 1.12 to 1.14. Figure 1.12 shows the analog to Figure 1.11

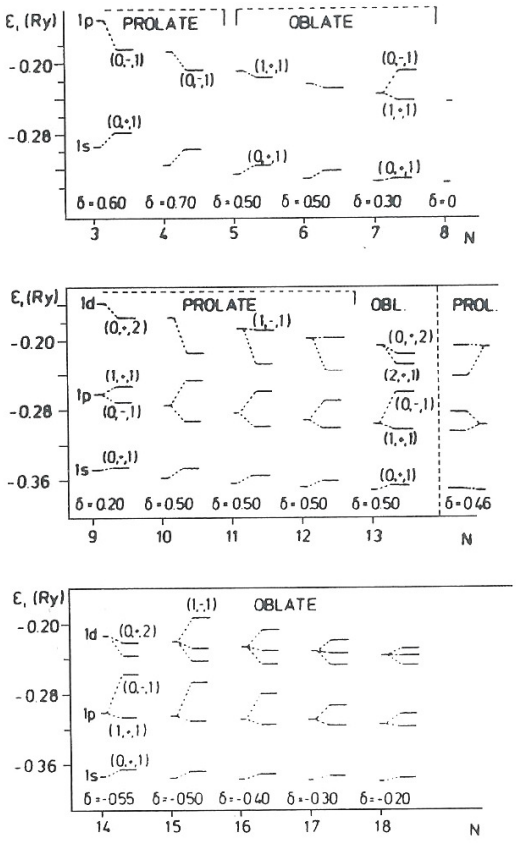

Figure 1.11 Evolution of the level structure as function of size N in the range $3 < N < 18$. In each case the deformation parameter δ, defined in Eq. (15), is given. For comparison, the spherical levels are also given. As one can see clearly, the spherical level structure is heavily perturbed in the midshell region. Note that in the case of $N = 18$ the cluster ends up with a spheroidal distortion (because of the interplay between 1d, and 2s levels). For $N = 13$, both prolate and oblate levels are given, because the two have a total energy, which is close (for the possibility of a three-axial distortion in this case, see [30]). Reproduced with permission from Reference [29]. Copyright 1988 by the American Physical Society

(spherical to spheroidal behavior). Figure 1.13 gives the second energy difference Δ_2 defined as:

$$\Delta_2(E) = E_{N+1} - (E_N + E_1) - (E_N - (E_{N-1} - E_1)). \tag{17}$$

As has been shown [27], this quantity is decisive for the mass abundances observed experimentally in a supersonic beam experiment. Finally, we show in Figure 1.14 the ionization potentials obtained within the spheroidal jellium model. Note that there is a pronounced odd–even alternation, as in the abundances, and that this effect is purely electronic and *produced without regard to the spin of the electrons and also without any pairing effects*

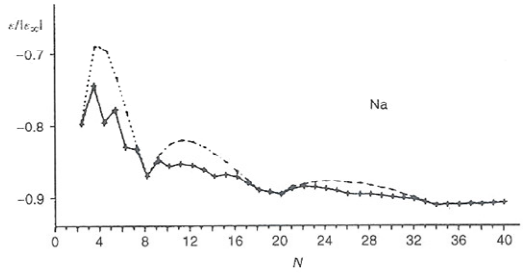

Figure 1.12 Energy per particle in units of $|\varepsilon_\infty|$. The solid line shows the data from the spheroidal jellium model, the dashed line the corresponding data from the spherical jellium model. The results are for $N < 41$. Reproduced with permission from Reference [29]. Copyright 1988 by the American Physical Society

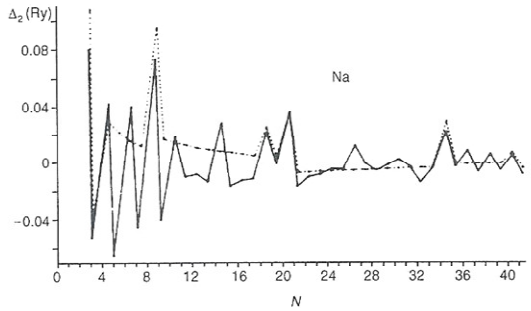

Figure 1.13 Second difference Δ_2 of the total energy as function of N. Solid line: distorted jellium; dashed line: spherical jellium. Reproduced with permission from Reference [29]. Copyright 1988 by the American Physical Society

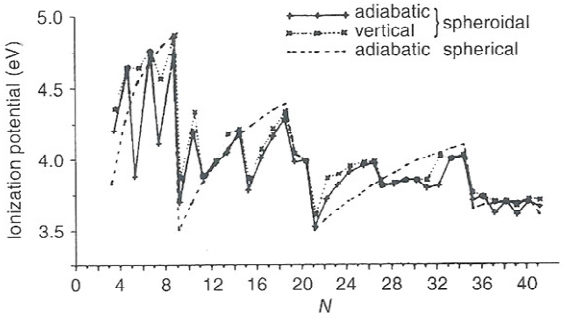

Figure 1.14 Ionization potential in various approximations. Note that the spherical sawtooth behavior is completely destroyed after allowing for spheroidal distortions. Originally it was believed that the strong odd–even alternation was related to the spin of the electrons. But, as shown first by the first author [29], it is a *kinematic* orbital effect. Reproduced with permission from Reference [29]. Copyright 1988 by the American Physical Society

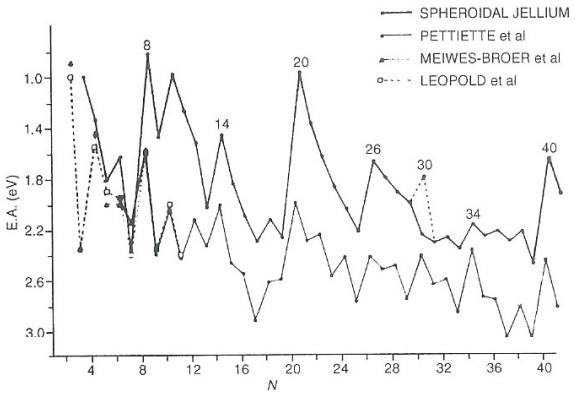

Figure 1.15 Comparison of the electron affinity within the spheroidal jellium model plus SIC and various experimental results (circles [44], triangles [45], squares [46]). For $N = 30$ theory predicts two isomers (prolate and oblate), which are nearly degenerate. But both do have different affinities and in the beam the signal will come from those clusters having the lower affinities (connected by dashed lines). Clearly, shell effects are very pronounced. Qualitatively theory and experiment agree rather well. In order to achieve *quantitative* agreement one has to introduce pseudopotential perturbation theory as sketched above. Reproduced by permission of Springer Verlag

as in nuclear structure theory. As explained in detail in [29] it is on the contrary an effect of the permanent change of level ordering and occupation as a function of N.

In addition we have calculated the electron affinities within the jellium model. But, as well known from experience in atomic physics, the LDA functional has to be corrected for so-called *self-interaction* effects (SIE) as originally proposed by Perdew and Zunger [8]. As explained in detail below, this leads to an orbital-dependent Kohn–Sham potential by the replacement [31]:

$$V_{\mathrm{SIC}}^{\mathrm{eff}} = V_{\mathrm{LDA}}^{\mathrm{eff}} - \delta_i. \tag{18}$$

Here i is the level in question and the functional δ_i is the self-interaction correction for the orbital i. We follow Perdew and Zunger [8] in writing

$$\delta_i = U_{\mathrm{es}}[n_i] + U_{\mathrm{xc}}^{\mathrm{LDA}}[n_i]. \tag{19}$$

Here the first part is the electrostatic self-Coulomb interaction and the second part is the analog correction for the exchange–correlation part of the effective potential. Please note that both functionals depend on the *total* density n_i and *not* on the spin densities as in the case of Perdew and Zunger who corrected the LSDA (Local Spin Density Approximation). Results for Cu are reproduced in Figure 1.15 [31]. Though with this simple functional quantitative agreement with experimental data is not to be expected, the experimentally observed shell effects in the electron affinity are qualitatively well reproduced.

1.3 THE OPTICAL PROPERTIES

In the following we describe the optical properties of metal clusters within the jellium model. We begin by introducing the TDLDA (time-dependent local density approximation)

to general TDDFT (time-dependent density functional theory) as was done *intuitively* by A. Zangwill and P. Soven in their seminal work [32]. The rigorous proof of this method was provided later by E. K. U. Gross and collaborators in a series of papers. For a rigorous derivation of this TDLDA (in this context sometimes called ADLDA (adiabatic local density approximation), which points to the range of validity of the TDLDA), the interested reader is referred to [33]. We continue with the intuitive introduction of the TDLDA.

We start by translating Fermi's golden rule concerning the photoabsorption into the language of density functional theory. If the jellium cluster is exposed to an external photon field $V_{\text{ext}}(\boldsymbol{r}, t)$ an induced charge density is set up, which is given as

$$\rho_{\text{ind}}(\boldsymbol{r},\omega) = \int \mathrm{d}\boldsymbol{r}'\chi(\boldsymbol{r}, \boldsymbol{r}'; \omega)V_{\text{ext}}(\boldsymbol{r}'; \omega). \tag{20}$$

In this equation χ is the *exact* dynamical density–density correlation function calculated with the inclusion of all many-body effects. As one can show [5], the exact χ is determined by solving the TDLDA integral equation

$$\chi(\boldsymbol{r}, \boldsymbol{r}'; \omega) = \chi^0(\boldsymbol{r}, \boldsymbol{r}'; \omega) + \int \mathrm{d}\boldsymbol{r}'' \,\mathrm{d}\boldsymbol{r}'''\chi^0(\boldsymbol{r}, \boldsymbol{r}''; \omega)K(\boldsymbol{r}'', \boldsymbol{r}''')\chi(\boldsymbol{r}''', \boldsymbol{r}'; \omega). \tag{21}$$

The so-called residual interaction $K(\boldsymbol{r}, \boldsymbol{r}')$ is defined (in Rydberg atomic units) as

$$K(\boldsymbol{r}, \boldsymbol{r}') = \frac{2}{|\boldsymbol{r} - \boldsymbol{r}'|} + \frac{\mathrm{d}}{\mathrm{d}\rho}V_{\text{xc}}[\rho(\boldsymbol{r})]\delta(\boldsymbol{r} - \boldsymbol{r}'). \tag{22}$$

The first part of the residual interaction K is the Coulomb potential established by the induced charge density $\rho_{\text{ind}}(\boldsymbol{r}, \omega)$ and the other part is the exchange–correlation contribution to the induced effective field. Whereas Zangwill and Soven [32] introduced this part intuitively without exact proof for the existence of this functional (for time-dependent densities), Gross was able to show [33] the restrictions on $V_{\text{xc}}(\boldsymbol{r}, t)$ and the assumptions to be made, to make this procedure an accurate one. To be brief, the procedure is valid if the system is at time t_0 in its non-degenerate ground state and if the external potential has a Taylor expansion in time around t_0. But the formulation of Gross is much more general; the interested reader should read the original papers by Gross.

Finally, the independent particle susceptibility $\chi_0(\boldsymbol{r}, \boldsymbol{r}'; \omega)$ is defined (see [5]) in terms of the one-particle Kohn–Sham eigenfunctions $\phi_i(\boldsymbol{r})$ and the retarded Green's function G of the Kohn–Sham Hamiltonian,

$$\chi^0(\boldsymbol{r}, \boldsymbol{r}'; \omega) = \sum_i^{\text{occ}} \phi_i^*(\boldsymbol{r})\phi_i(\boldsymbol{r}')G(\boldsymbol{r}, \boldsymbol{r}'; \varepsilon_i + \hbar\omega) + \text{c.c.}(\omega \to -\omega). \tag{23}$$

Whereas the full density–density correlation function contains many-body effects (as collective excitations (as poles)), χ_0 does *not* contain these features. It is by construction an independent particle function. As such it is the response function to the total perturbing effective field,

$$\rho_{\text{ind}}(\boldsymbol{r}, \omega) = \int \mathrm{d}\boldsymbol{r}'\chi^0(\boldsymbol{r}, \boldsymbol{r}'; \omega)V_{\text{eff}}(\boldsymbol{r}', \omega), \tag{24}$$

with the effective potential defined as

$$V_{\text{eff}}(\boldsymbol{r}, \omega) = V_{\text{ext}}(\boldsymbol{r}, \omega) + \int \mathrm{d}\boldsymbol{r}'K(\boldsymbol{r}, \boldsymbol{r}')\rho_{\text{ind}}(\boldsymbol{r}', \omega). \tag{25}$$

In Eq. (25) all many-body effects are implicitely contained in the effective field. The interesting point to note is that also in the presence of a *time-dependent field all* many-body effects can be stored in a local one-particle potential, to which the electrons respond as *independent* particles.

Once χ is determined we are ready to calculate the photoabsorption cross-section $\sigma(\omega)$ (for a detailed derivation of these formulas see [5]):

$$\sigma(\omega) = \frac{4\pi\omega}{c}\mathrm{Im}[\alpha(\omega)], \tag{26}$$

$$\alpha(\omega) = \int_0^\infty \mathrm{d}r\, r\alpha(r, \omega), \tag{27}$$

$$\alpha(r, \omega) = -\frac{4\pi}{3}r^2 \int_0^\infty \mathrm{d}r'\, r'^3 \chi_{l=1}(r, r'; \omega). \tag{28}$$

Here we have used spherical symmetry, which means that χ is diagonal in the angular momentum and that for the response to the photon field it is only the component with $l = 1$ we need to calculate. The last equation completes the formalism and we are ready to present the results for a number of jellium clusters.

We start with a typical result for jellium-cluster absorption in the range $100 \leq N \leq 200$, namely $N = 198$. In Figure 1.16 the dashed line gives $\mathrm{Im}[\alpha(\omega)]$. In comparison we show by a continuous line the absorption obtained within the Drude approximation to the dielectric constant $\varepsilon(\omega)$. Here the electrons are described as a system of damped 'oscillators' with eigenfrequency $\omega = 0$. For this reason there is no absorption feature beside

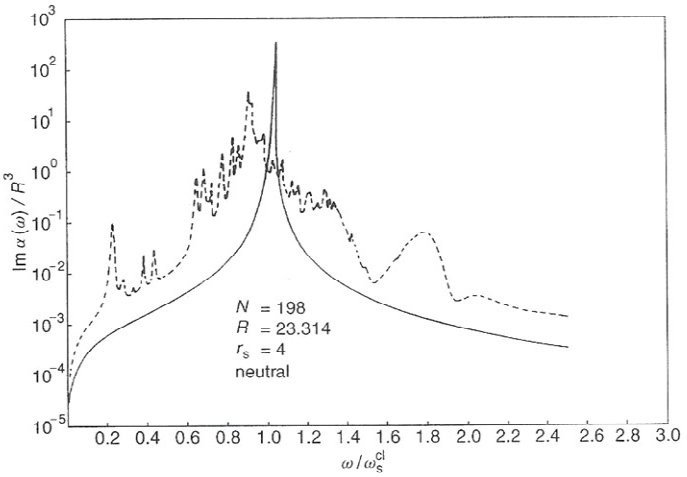

Figure 1.16 Imaginary part of the complex polarizability $\alpha(\omega)$ for an Na cluster with $N = 198$ in units of R^3. Effective single-pair excitations, as well as the surface plasmon and the volume plasmon, are clearly resolved. For comparison the result of the local Drude theory is also given. In this case there is only one mode of excitation, the classical surface-plasmon polariton or Mie-resonance at $\omega_p/\sqrt{3}$. Because the frequency is scaled with this frequency the Drude curve peaks trivially at 1. For more explanation see text. Reproduced with permission from Reference [5]. Copyright 1985 by the American Physical Society

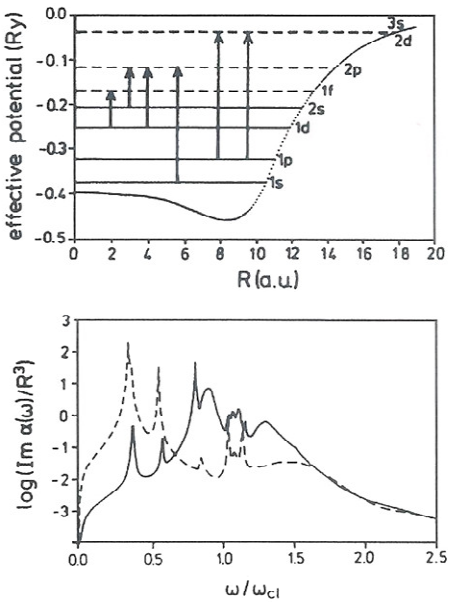

Figure 1.17 Dipole-allowed absorption in jellium Na_{20} and its interpretation. The continuous line gives the result from the TDLDA. The nature of the double structure between 0.5 and 1.0 can be understood in two steps. First, the TDLDA is compared with LDA, the independent-particle response (dashed line). Each peak corresponds to one arrow in the upper part of the figure. After turning on the *interaction* among excited pairs, bare pairs are transformed into dressed pairs. Note that there is a one-to-one correspondence between the spikes in the two curves. As explained in the text there is another effect of this interaction, namely the formation of a collective surface mode at about 0.9. This feature has *no* counterpart in the dashed curve. Furthermore there is one more collective effect at about 1.2. For more explanation see text. Reproduced with permission from Ekardt, Pacheco and Schone, *Comments on Atomic and Molecular Physics*, **31**, 291 (1995). Copyright by OPA (Overseas Publishers Association) B.V

the collective surface plasmon–polariton. Quantum-mechanically there are a number of dipole-allowed single-particle transitions (see Figure 1.17). But, remarkably enough, these transitions are *very* weak. So the quantum corrections are weak in general and consist in the appearance of two kinds of transitions in addition to the classical Mie plasmon at $\omega_s = \omega_p/\sqrt{3}$, namely the various particle–hole transitions (the tiny spikes) and the broad hump at ω_p which is the precursor to the volume plasmon. The plasmon frequency ω_p is given by $\omega_p^2 = 4\pi ne^2/m$. For *smaller* particle numbers this picture changes gradually. This is demonstrated by Figure 1.17, showing the calculated absorption spectrum for Na_{20} within the jellium model. In order to better identify the origin of the various spikes (single-particle transitions) we show in the upper panel the level structure of occupied (continuous line) and empty levels (dashed lines). The arrows mark allowed optical transitions in this potential. Clearly, there is a one-to-one correspondence between the arrows in the upper part and the spikes in the *dashed* curve, describing the absorption within the independent-particle approximation (i.e. *without* many-body effects). Those effects can be clearly identified by comparing the absorption at the TDLDA level (continuous line) with

the dashed line. Upon taking into account many-body effects all naked particle–hole pairs are transformed to dressed ones. In addition to these effects there are two more features, one slightly below the classical Mie frequency and the second at about $1.2\,\omega_p$. The former is the surface plasmon and the latter is a complicated collective feature, already known from flat surfaces [51]. These two collective features gain oscillator strength at the cost of low-lying single pairs which are of reduced strength in the interacting system. In addition to these quantum effects, there is a *purely classical* effect, already known from the classical damped oscillator; if a damped oscillator is driven by an external field of frequency below its resonance frequency, it oscillates *in phase* with the external field. But if the external frequency is above resonance there is a phase shift by π.

This general statement applied to the problem in question means: the surface plasmon in the interacting system screens very efficiently the external electric field for all frequencies ω below ω_s. This leads to a further reduction of the oscillator strength of the single pair lines below the surface plasmon. This means the external field is *screened*. In contrast, at frequencies above ω_s the external field is *antiscreened*, which means enhanced! Indeed, for all frequencies above the surface-plasmon frequency the intensity of the independent particle lines (dashed line) is *enhanced*, a feature which is clearly seen in Figure 1.17. The remarkable feature of the absorption in Na_{20} is that there is not a single surface-plasmon line but a doublet. This behavior is called *Landau fragmentation* because it is the analog (for a discrete level structure) to Landau damping (coupling of the plasmon to a *continuous* single-particle spectrum). Remarkably enough, the jellium picture provides for Na_{20} a reliable, though oversimplifying, description of photoabsorption. The reason for this is discussed in the following section.

1.4 PSEUDOPOTENTIAL PERTURBATION THEORY

For a better understanding of the range of validity of the jellium model and in order to learn how it can be successively improved we discuss in the following the specific example of Na_8. A molecular dynamics study gives three different low-lying isomers (see Figure 1.18) with D_{2d} being the ground state within the Car–Parrinello pseudopotential plane-wave method [34]. Because Na has only very weak non-local components in the *ab initio* pseudopotentials we can use *local* pseudopotentials of the Heine–Abarenkov type [35]. As long as we are interested in the dynamical properties of the loosely bound valence electrons a pseudopotential description is perfectly adequate (for a tractable method for transition metals see below). With these restrictions, the cluster electrons are moving in an external potential of the type

$$v_{\text{ext}} = \sum_{i=1}^{N} v_{\text{ps}}(\boldsymbol{r} - \boldsymbol{R}_i). \tag{29}$$

Here the pseudopotentials v_{ps} are located and are spherically symmetric around the ionic sites $\boldsymbol{R}_i$. In order to better understand the performance of the jellium model each of these potentials is decomposed into its various angular parts with respect to an arbitrary cluster 'center', which we assume to be the center of mass (for a discussion of other 'centers' see [36]),

$$v_{\text{ps}}(\boldsymbol{r} - \boldsymbol{R}_i) = \sum_{l=0}^{\infty} \sum_{m=-l}^{+l} \frac{\sqrt{4\pi}}{2l+1} \alpha_l(R_i, r) Y^*_{l,m}(\Theta_i, \Phi_i) Y_{l,m}(\theta, \phi). \tag{30}$$

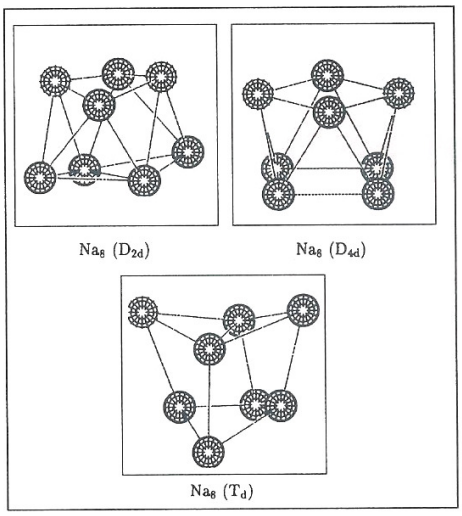

Figure 1.18 Geometries of the three lowest isomers of Na_8 as obtained from Car–Parrinello calculations [34, 47]

Now we have to perform the total sum over all ionic sites in order to get the total potential. Hence we get the total spherical part of the potential as

$$v_0^{\text{ext}}(r, R) = \frac{1}{4\pi} \sum_i \alpha_{l=0}(R_i, r). \tag{31}$$

Please note that this part depends on (the modulus) of *all* ionic sites $\boldsymbol{R}_i$. The remaining part of the external potential contains geometrical information and effects finally the transition from the molecular structure (for few ionic numbers) to the solid (for a large number of ions). As we shall see in a number of examples the first, spherically symmetric part of the pseudopotential is *extremely well* represented by the jellium model and is by far the largest contribution to the total potential. Therefore the second part, containing the geometrical information, can be treated by perturbation theory.

To be specific we consider in what follows the example of Na_8. According to the Car–Parrinello method [34] there are three low-lying isomers (see Figure 1.18) with D_{2d} being the ground state followed by two structures with a slightly higher total energy. Note in passing that quantum chemists, with their methods, find T_d to be the ground-state symmetry. As we shall see below there exists the possibility via photoabsorption to determine the geometrical structure of a cluster. For this purpose we have to study the influence of the geometrical part of the total potential on the absorption. This is done by first investigating the spherical potential part of Na_8 in the D_{2d} structure which is shown in the left-hand panel of Figure 1.19. Note that it is almost identical to the spherical jellium model potential discussed before. In this way we have a justification for its use in the case of the magic-number clusters $N = 8$, 20, 40, 58, 92, 138, etc. The two most important *nonspherical* potential parts are shown in the right-hand panel of Figure 1.19. Their influence is studied via perturbation theory. The result is as expected: very small changes in the single-particle energies, which are now split according to the point group of the

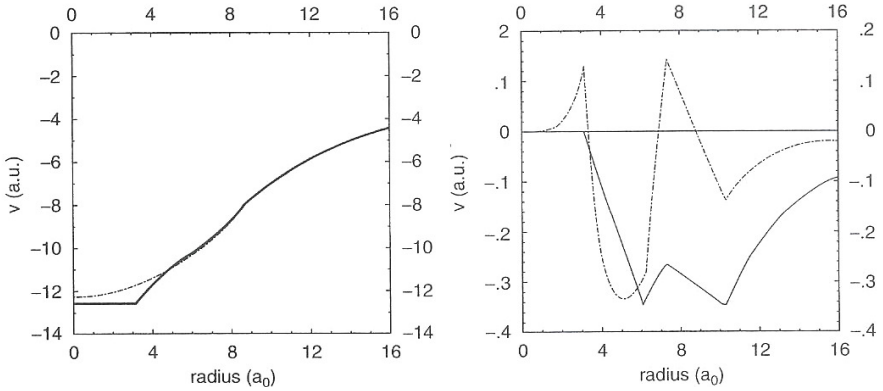

Figure 1.19 Various potential components resulting from Eq. (30) for the ground state of Na_8. The left-hand panel shows the spherical component (Eq. (31)) given by the continuous line. For comparison the spherical jellium potential (dashed line) is also given. As one can see the two are almost identical and much larger than the two most important nonspherical potential parts $v_{l=2,m=0}(r)$ (continuous line) and $v_{l=4,m=0}(r)$ (dashed line) displayed in the right-hand panel. Note that these two components are strongly fluctuating compared to the smooth spherical part. These potential parts make the optical response different in the three isomeric states. In the end they are responsible for the transition from the molecule with a point-group symmetry to the solid with a space-group symmetry — a problem that has not yet been solved

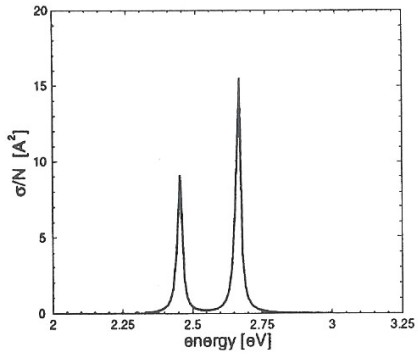

$Na_8(D_{2d})$

Figure 1.20 Optical absorption of Na_8 in its ground-state structure D_{2d}. This result from pseudopotential perturbation theory is explained in the main text. The spherical plasmon line at about 2.5 eV (see Figure 1.21) is split into two components which can be understood as follows. The moments of inertia of the structure D_{2d} point to a prolate spheroid within the jellium approximation to the distribution of ions. In such a system there are two collective excitations: one at higher frequencies (perpendicular to the axis of symmetry) and one for the motion along the axis of symmetry. Because the motion perpendicular is twofold degenerate its intensity is twice that of the low-frequency motion (with the cluster being statistically oriented in the beam (see [30])

cluster. More interesting is the effect of the geometry on the optical absorption. This effect is investigated and described in detail in [37] (essentially the TDLDA integral equation for $\chi(\boldsymbol{r}, \boldsymbol{r}'; \omega)$ is solved perturbatively). The result for Na_8 in its ground-state structure D_{2d} is shown in Figure 1.20. The result is unexpected and can hardly be understood within the jellium approximation to the external potential, namely the moments of inertia for the actual cluster structure point to a *prolate spheroid.* The spherical one-component surface plasmon is split into two components, with the high-frequency line about twice as intensive as the low-frequency line. This is because the fast oscillation perpendicular to the axis of symmetry is twofold degenerate. This result is unexpected because within the jellium approximation to the external potential the sphere is stable against deformations to a spheroid! The result is not only unexpected, but also annoying, because the *two*-peak structure seems to contradict the experimental findings of a broad one-peak hump centered around 2.5 eV. Before we can make a final decision about the relevance of our calculations, we present in the next figure absorption spectra of the other isomers. The upper part in Figure 1.21 shows the D_{4d}, whereas the lower part shows the T_d structure. Each is essentially a one-peak structure with the right position at about 2.5 eV. As we shall see later it is nevertheless the D_{2d} structure that is in agreement with the experiment — after taking into account the effects of temperature which we discuss next.

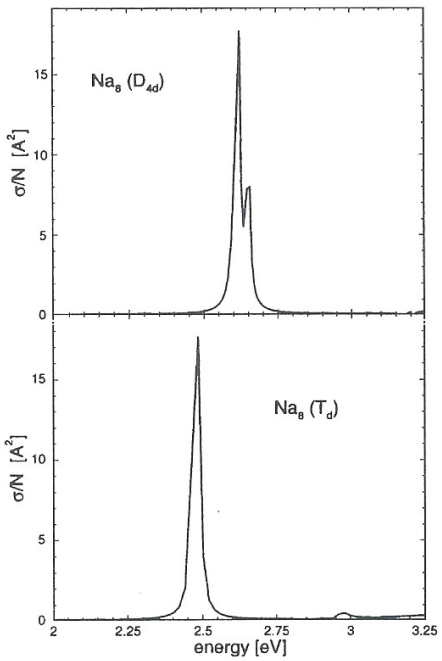

Figure 1.21 Same as Figure 1.20 for the other two structures of Na_8. The interpretation parallels the one for the D_{2d} symmetry. The absorption in Na_8 in the D_{4d} structure (upper panel) points to an *oblate* spheroid. Therefore the low-frequency component is twice as intensive as the high-frequency one. Finally, the T_d structure is almost spherical; therefore the absorption consists of *one* peak positioned at the spherical jellium line

1.5 THE EFFECT OF TEMPERATURE

Since most absorption spectra are taken at elevated temperatures T, the theoretical prediction should not be made for $T = 0$, but for $T > 0$. At higher temperatures the ions are oscillating around their equilibrium positions. For this reason the *measured* cross-section is an ensemble average over the canonical ensemble at temperature T,

$$\langle \sigma(\omega) \rangle = \frac{1}{Z} \sum_i \sigma(\omega; \boldsymbol{R}_i) \mathrm{e}^{-\beta E[\boldsymbol{R}_i]}, \tag{32}$$

where Z is the partition function

$$Z = \sum_i \mathrm{e}^{-\beta E[\boldsymbol{R}_i]}, \quad \beta = \frac{1}{kT}. \tag{33}$$

Here the canonical phase-space sampling is performed via the Monte Carlo method (for details see [6]). As the cluster in the beam is oriented statistically, we have to perform three different calculations,

$$\langle \sigma_{\mathrm{av}}(\omega) \rangle = \frac{1}{3} \sum_{i=x,y,z} \langle \sigma_i(\omega) \rangle. \tag{34}$$

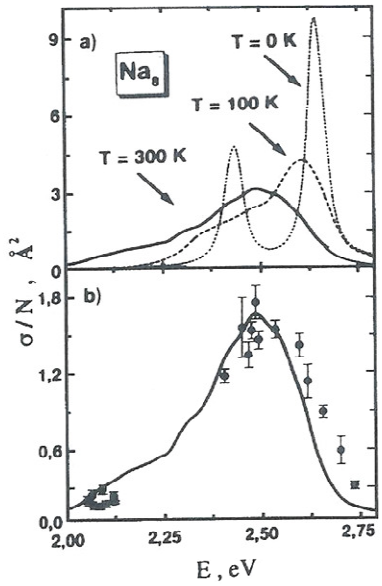

Figure 1.22 (a) Line shape of the photoabsorption cross-section of Na_8 at three different vibrational temperatures in its ground-state structure D_{2d} according to Eqs (32)–(34). A numerical damping of 0.02 eV has been assumed at $T = 0$ K. This curve is without ionic fluctuations; the other two contain ionic fluctuations at the corresponding temperatures 100 K and 300 K.
(b) Comparison with the experimental data of the Berkeley group [48]. The theoretical curve (solid line) has been renormalized in order to exhaust 55% of the Thomas–Reiche–Kuhn sum rule (f-sum rule) in accord with the experimental findings

Now we have a picture about how demanding temperature-dependent calculations are: we need at each T and $\omega 10^4$ Monte Carlo points and 10^2 frequencies in order to cover the experimental range. Furthermore we need the three different directions x, y and z. So we had to solve three million times the TDLDA integral equation with full inclusion of the ionic structure (via pseudopotential perturbation theory). Needless to say it seems almost impossible to perform calculations of this type for transition metals with the additional complication of the d-electrons!

The result of the Monte Carlo canonical sampling of the phase space is presented in Figure 1.22. At zero temperature, we reproduce the pronounced doublet, which seems to disagree with the experimental finding of a broad one-peak structure. With elevated temperature the two peaks merge into one and almost agree with the experimental data at 300 K, resolving a long-standing puzzle. The *observed* width of the surface-plasmon line is not related to dissipative processes or to Landau damping (coupling to particle–hole pairs), nor is it due to electron–phonon coupling. It is instead a line-broadening, due to the oscillations of the ions around their equilibrium positions.

We conclude with two more examples which demonstrate the power of pseudopotential perturbation theory. Figure 1.23 shows the geometry and absorption spectra of Na_6 which

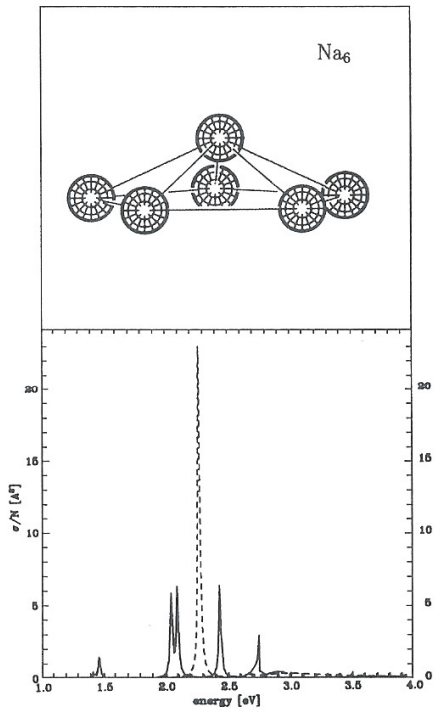

Figure 1.23 Geometry (upper panel) and optical absorption (lower panel) of Na_6 in its ground state C_{5v} [34]. The spherical jellium line (dashed curve) disintegrates into various particle–hole lines (continuous curve) under the influence of the strongly fluctuating potential components shown in the next figure. The continuous curve agrees *qualitatively* with results obtained by quantum chemists [49]

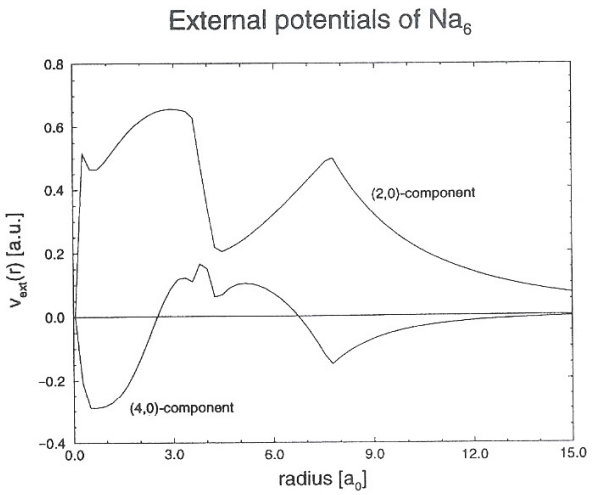

Figure 1.24 The most important nonspherical potential components of Na_6 in the geometry C_{5v}. Because these components are heavily fluctuating and *not* small, there is *no* collective peak at the TDLDA level

is an open-shell cluster (pentagonal pyramid). The dashed line is the result of the spherical jellium calculation; it shows one collective peak. Under the influence of the *strong and strongly fluctuating* nonspherical parts of the potential (shown in Figure 1.24) the efficient Coulomb coupling of (excited) particle–hole pairs is destroyed and the plasmon *disintegrates* into its constituent components. In the last example we show in Figure 1.25 the absorption spectra of Na_{90}. Because for such large clusters *ab initio* studies of the equilibrium structure do not exist we just built small crystal fractions of fcc, bcc, hcp and icosahedral symmetry and calculated the total energy within second-order pseudopotential perturbation theory (the first-order contribution is identical to zero for symmetry reasons). In the case of Na_{90} it is the hcp structure that is energetically favorable. Accurate experimental data on Na_{90} do not exist. First preliminary data confirm a peak on the high-energy side [38].

1.6 SUMMARY AND CONCLUSIONS

The alert reader will have realized that almost all examples given in this chapter are from Na. Of course this was on purpose: two of the most important conditions to be fulfilled for the excellent validity of the jellium model, namely (a) that the pseudopotential is local and (b) that the 'geometrical' parts of the ionic arrangement are weak, are best met in Na_N. In trying other elements we found only *one* other material that works comparably well — potassium. But the important point to note is that this simple model serves as a guideline for more complex cases. After electronic shells and plasmons have been found in Na, they have been found in almost all metal clusters. In order to get the same quantitative agreement as in the case of Na one has either to do all-electron calculations or to use non-local pseudopotentials, as has been done in the case of Li [39, 40]. But in these

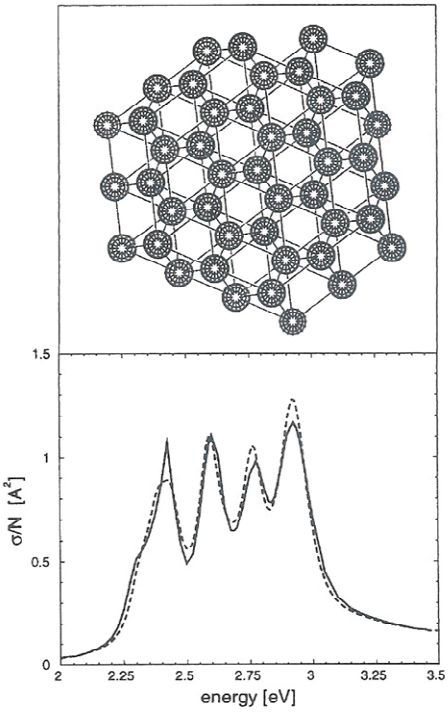

Figure 1.25 Geometry and optical absorption of Na_{90}. For $N = 90$ there are no determinations of the geometry at the *ab initio* level available. We have therefore simply calculated the total energy within pseudopotential perturbation theory of second order for various model clusters built as small crystal fractions of fcc, bcc, hcp and icosahedral type. For the case in question the hcp structure (see upper part of the figure) has the lowest total energy

calculations the geometrical part of the (non-local) pseudopotentials has not been studied. Only the spherical component has been modified and this results in just another position of the plasmon line and not in a qualitative change of the spectra. This is not sufficient to catch the full variety of metal-cluster absorption. For instance, the disintegration of plasmons in Na_6 is a new and qualitative aspect that can be obtained only in a model *beyond* the spherical average of the potential. This has never been done for *ab initio* pseudopotentials.

Another important point of complications is the existence of d-electrons. Though the noble metals, like the alkaline metals, show magic numbers [30], indicating that the d-electrons do not sufficiently strongly disturb the mutual correlation of the s-electrons (which is the root of the occurrence of shells), they do couple dynamically to the s-electrons, as is already known from the bulk crystals of the noble metals [13, 18]. For these cases we need a new and much more complicated theory. This is *ab initio* TDLDA [41, 42] which is currently being constructed. Here, we calculate the electronic

structure *ab initio* at the all-electron level, within the FPLAPW method (full potential linearized augmented plane wave method; computer code WIEN95 [43]). In this way, the *dynamical* coupling between s- and d-electrons is taken into account from the very beginning. In the case of clusters an additional complication occurs, namely *hybridization* (e.g. in Ag_n the 4d- and 5s-electrons hybridize). This feature is hardly caught by any jellium-type model.

From a general point of view the example of the temperature-dependent absorption in Na_8 is of the utmost importance. Because the method TDLDA, which was introduced intuitively in the seminal work by Zangwill and Soven [32], has itself been doubted for several years. But as we know from the work of Gross's group this method is on a firm theoretical basis and should deliver exact results whenever the residual interaction is not frequency-dependent and is of the plasmon type. In the case of excitons it will fail, because here the screening in the Coulomb part of the residual interaction is essential. Therefore it is not surprising that all applications of the TDLDA to atoms, molecules and clusters and to solids are in a frequency region where no excitons are to be expected, i.e. the spectral region *above* the particle–hole part of the excitations but *not* that below it.

1.7 REFERENCES

[1] D. Pines and P. Nozières, *The Theory of Quantum Liquids*, W. A. Benjamin, New York, 1966.
[2] N. D. Lang, 'The density functional formalism and the electronic structure of metal surfaces', in *Solid State Physics, Vol. 28*, ed. H. Ehrenreich, F. Seitz and D. Turnbull (Academic Press, New York, 1973), p. 225.
[3] W. Ekardt, *Phys. Rev. B* **29**, 1558 (1984).
[4] H. Nishioka, K. Hansen and B. Mottelson, *Phys. Rev. B* **42**, 9377 (1990).
[5] W. Ekardt, *Phys. Rev. Lett.* **52**, 1925 (1984); *Phys. Rev. B* **31**, 6360 (1985).
[6] J. M. Pacheco and W.-D. Schöne, *Phys. Rev. Lett.* **79**, 4986 (1997).
[7] W.-D. Schöne, W. Ekardt and J. M. Pacheco, *Phys. Rev. B* **50**, 11079 (1994).
[8] A. Zunger and J. M. Perdew, *Phys. Rev. B* **23**, 5048 (1981).
[9] Z. Penzar and W. Ekardt, *Z. Phys. D* **17**, 69 (1990).
[10] J. M. Pacheco and W. Ekardt, *Ann. Physik* **1**, 254 (1992).
[11] W. Schulze, P. Frank, K.-P. Charlé and B. Tesche, *Berichte Bunsenges. Phys. Chem.* **88**, 263 (1984).
[12] L. D. Landau and M. Lifschitz, *Electrodynamics of Continuous Media*, Pergamon Press, Oxford, 1960.
[13] D. Pines, *Elementary Excitations in Solids*, Benjamin, New York, 1964.
[14] N. D. Lang and W. Kohn, *Phys. Rev. B* **1**, 4555 (1970); *Phys. Rev. B* **3**, 1215 (1971).
[15] A. G. Eguiluz, *Phys. Rev. B* **35**, 5473 (1987).
[16] R. N. Barnett, U. Landman and C. L. Cleveland, *Phys. Rev. B* **27**, 6834 (1983).
[17] K.-P. Charlé, L. König, S. Nepijko, I. Rabin, and W. Schulze, *Cryst. Res. Technol.* **33**, 7 (1998).
[18] H. Raether, *Plasmons*, Springer, Berlin, 1980.
[19] *EXAFS, Basic Principles, and Data Analysis*, Springer, Berlin, 1994.
[20] P. Hohenberg and W. Kohn, *Phys. Rev.* **136**, B864 (1964).
[21] W. Kohn and L. J. Sham, *Phys. Rev.* **140**, A1133 (1965).
[22] O. Gunnarsson and B. I. Lundqvist, *Phys. Rev. B* **13**, 4274 (1976).
[23] S. Bjørnholm, J. Borggreen, O. Echt, K. Hansen, J. Pedersen and M. P. Rasmussen, *Phys. Rev. Lett.* **65**, 13 (1990).
[24] W. D. Knight, K. Clemanger, W. A. de Heer, W.A. Saunders, M. Y. Choi and M. L. Cohen, *Phys. Rev. Lett.* **52**, 2141 (1984).
[25] T. P. Martin, T. Bergmann, H. Goehrlich and T. Lange, *Z. Phys. D* **19**, 25 (1991).